Micro-organization and visco-elasticity of the interphase nucleus revealed by particle nanotracking

Yiider Tseng[1], Jerry S. H. Lee[1], Thomas P. Kole[1], Ingjye Jiang[1] and Denis Wirtz[1,2,3,*]

[1]Department of Chemical and Biomolecular Engineering, [2]Department of Materials Science and Engineering, [3]Graduate Program in Molecular Biophysics, The Johns Hopkins University, Baltimore, 3400 N. Charles Street, MD 21218, USA

*Author for correspondence (e-mail: wirtz@jhu.edu)

Accepted 5 January 2004
Journal of Cell Science 117, 2159-2167 Published by The Company of Biologists 2004
doi:10.1242/jcs.01073

Summary

The microstructure of the nucleus, one of the most studied but least understood cellular organelles, is the subject of much debate. Through the use of particle nanotracking, we detect and quantify the micro-organization as well as the viscoelastic properties of the intranuclear region in single, live, interphase somatic cells. We find that the intranuclear region is much stiffer than the cytoplasm; it is also more elastic than viscous, which reveals that the intranuclear region displays an unexpectedly strong solid-like behavior. The mean shear viscosity and elasticity of the intranuclear region of Swiss 3T3 fibroblasts are 520 Poise (P) and 180 dyn/cm^2, respectively. These measurements determine a lower bound of the propulsive forces (3-15 picoNewton) required for nuclear organelles such as promyelocytic-leukemia bodies to undergo processive transport within the nucleus by overcoming friction forces set by the intranuclear viscosity. Dynamic analysis of the spontaneous movements of nanospheres embedded in the nucleus reveals the presence of putative transient nuclear microdomains of mean size 290±50 nm, which are mostly absent in the cytoplasm. The strong elastic character and micro-organization of the intranuclear region revealed by particle nanotracking analysis may help the nucleus to preserve its structural coherence. These studies also highlight the difference between the low interstitial nucleoplasmic viscosity, which controls the transport of nuclear proteins and molecules, and the much higher mesoscale viscosity, which affects the diffusion and directed transport of nuclear organelles and re-organization of interphase chromosomes.

Movies available online

Key words: Nucleus, Nuclear organization, Particle tracking, Microrheology, Cajal body, PML body

Introduction

The micro-organization of the nucleus is the subject of much debate (Lamond and Earnshaw, 1998; Pederson, 2002). One view describes the nucleus as a mostly disorganized, fluid-like viscous bag containing transient structures such as transcribing and replicating chromosomal segments, nucleoli and nuclear organelles (Cajal bodies, etc.), which form and dissociate relatively rapidly (Lamond and Earnshaw, 1998). This model is supported by recent efforts using time-resolved microscopy that show the dynamic behavior of chromatin in interphase nuclei (Gasser, 2002). Another view describes the nucleus as a compartmentalized region, which contains its own extended nucleoskeleton (Luby-Phelps et al., 1986; Nickerson, 2001). This skeletal architecture is believed to provide mechanical support for the chromosomes and for the large protein complexes involved in replication and transcription of DNA. The development of time-lapse microscopy in live cells has helped us change our view of the interphase nucleus from a static structure, containing immobile chromosomes and macromolecular assemblies confined to fixed nuclear compartments, to that of an extremely dynamic organelle (Carmo-Fonseca, 2002; Pederson, 2002; Phair and Misteli, 2000).

Fluorescence recovery after photobleaching (FRAP) analysis suggests that the movements of small solutes and proteins in the nucleus of mammalian cells are extremely rapid (Phair and Misteli, 2000). Microinjected 500-750 kDa dextran has a diffusion coefficient in the nucleus which is only 3-5 times lower than in water (Lukacs et al., 2000; Seksek et al., 1997). Similarly, the transport of green fluorescence protein (GFP) is fast. GFP takes seconds to travel distances equal to the size of the mammalian cell nucleus (Li et al., 2003; Phair and Misteli, 2000). While slower than GFP, the transport of GFP fusion nucleosomal-binding protein HMG-17, pre-mRNA splicing factor SF2/ASF and the rRNA processing protein fibrillarin can be entirely described as a hit-and-run mechanism, composite of fast diffusion interrupted by transient binding of these proteins to their respective, immobile nuclear compartments (Phair and Misteli, 2000). The transport of these GFP fusion proteins is independent of energy, indicating that these proteins use a passive, purely Brownian mechanism of movement (Phair and Misteli, 2000). Similarly, FRAP and fluorescence correlation spectroscopy show that fluorescein-labeled oligodeoxynucleotides diffuse in the nucleus as rapidly as in aqueous solutions (Politz et al., 1998; Politz et al., 1999; Politz et al., 2000). By contrast, FRAP analysis suggests that GFP-fusion proteins of histones H2B and H3 (Li et al., 2003; Phair and Misteli, 2000) and microinjected DNA fragments (Lukacs et al., 2000) are immobile in the nucleus, presumably because of their tight association with chromatin, which is

itself immobile. Together, these results suggest that the intranuclear region is only slightly more viscous than water and that the apparent slower motion of nuclear proteins can be accounted for by strong, but transient, interactions to seemingly immobile nuclear structures.

The intranuclear diffusion of inert polymers with a molecular mass >750 kDa is significantly slower than indicated by classical diffusion theory, which predicts that the diffusion coefficient of a polymer is inversely proportional to its hydrodynamic radius (Lukacs et al., 2000; Seksek et al., 1997). These larger polymers, which do not interact directly with subnuclear structures, must experience an enhanced viscosity, drastically slowing down their motion. Real-time fluorescence microscopy reveals that interphase chromosomes are dynamic and their movements can be decomposed into a fast component at early time-points (albeit slower than that of nuclear proteins) and a slower component at later time-points (Marshall et al., 1997; Vazquez et al., 2001). Similar approaches reveal that the motility of chromosomes is restricted and compartmentalized in the nucleus (Bornfleth et al., 1999; Cremer and Cremer, 2001; Edelmann et al., 2001). Complementary functional studies suggest that such dynamic and localized re-organization of interphase chromosomes is required for biological processes such as recombination (Marshall et al., 1997). Cajal bodies and promyelocytic leukemia (PML) bodies, submicron nuclear organelles that are involved in ribosome biogenesis and transcription, respectively, and are enriched in transcriptional regulators, undergo highly restricted motion in the nucleus (Muratani et al., 2002; Platani et al., 2002). The slow motion of chromosomes and organelles in the interphase nucleus might be due to their interactions with subnuclear structures and/or the same enhanced viscosity experienced by inert polymers in the nucleus. The speed of transport of chromosomes and nuclear organelles can be further reduced by the elasticity of the intranuclear region. Indeed, the mean squared displacement of latex beads in viscoelastic networks of chromosomal DNA (Goodman et al., 2002) increases more slowly with time because of the elasticity of those networks, which prevents free viscous diffusion.

Here, we present particle nanotracking analysis that demonstrates the viscoelastic nature and detects the micro-organization of the intranuclear region in live interphase cells. The viscoelastic properties of the intranuclear region explain the slow diffusion of Cajal bodies and helped us to estimate the minimum propulsive forces required for PML bodies to undergo directed motion within the nucleus. These studies highlight the fundamental difference between the low nucleoplasmic viscosity, which controls the diffusion of nuclear proteins and molecules, and the much higher mesoscale viscosity, which affects the transport of nuclear organelles and the large-scale, dynamic re-organization of chromatin.

Materials and Methods

Cell culture

Swiss 3T3 fibroblasts obtained from American Type Culture Collection (ATCC, Manassas, VA) were maintained at 37°C in a humidified environment containing 5% CO_2 in Dulbecco's Modified Eagle's Medium (DMEM) (ATCC) supplemented with 10% bovine calf serum (ATCC), following the manufacturer's protocol.

Microinjection, cell viability, and particle nanotracking microrheology

Nuclei of live cells were microinjected with yellow-green fluorescent, carboxylate-modified, 100-nm diameter nanospheres (Molecular Probes, Eugene, OR). These nanospheres were extensively dialyzed against Dulbecco's phosphate buffered saline (D-PBS) and subsequently diluted in D-PBS to a final concentration of ~10^{11} nanospheres/ml. This solution was filtered through a 0.22 μm filter and stored at 4°C. The nanospheres were microinjected using borosilicate microneedles and an Eppendorf Transjector 5246 (Brinkmann Instruments, Westbury, NY). The microneedles, which had an inner diameter of 0.3 μm and an outer diameter 0.4 μm (World Precision Instruments, Sarasota, FL), were loaded with 10 μl of the nanosphere solution using micropipettes (Brinkmann Instruments).

Cells were verified to be viable for at least 6 hours after microinjection using Trypan Blue (Sigma). After 6 hours of particle tracking, the tested cells were rinsed twice with balanced salt solution (BSS) and a diluted Trypan Blue solution (equal amounts of 0.4% Trypan Blue solution and BSS) was added to the dishes for 5 minutes. The tested cells were monitored whether they resisted any dye-uptake, an indication that cells are alive.

Movies of fluctuating fluorescent nanospheres, embedded in the nucleus and the perinuclear region of the cytoplasm, were recorded with a silicon-intensifier target (SIT) camera (Dage-MTI, Michigan City, IN) mounted on an inverted epifluorescence microscope (Nikon, Melville, NY) (Leduc et al., 1999). Displacements were monitored with a 100× Plan Fluor oil-immersion objective (NA 1.3) over a field of view of 150 μm×150 μm. Images of the nanospheres were analyzed by a custom particle-nanotracking routine incorporated into the image acquisition/analysis system Metamorph/Metaview (Universal Imaging, West Chester, PA) as described (Tseng and Wirtz, 2001). The displacements of the particles' centroids were monitored in the focal plane of the objective for 20 seconds at a frequency of 30 frames per second. Twelve nuclei were studied. The centroid of each nanosphere, defined as the intensity-weighted centroid of the nanosphere, was tracked with ≈5 nm resolution, as determined independently by immobilizing similar nanospheres with a strong adhesive on a glass coverslip and tracking their apparent displacements (Apgar et al., 2000). Individual time-averaged mean squared displacements (MSDs) $\langle \Delta r^2(\tau)\rangle = \langle [x(t+\tau)-x(t)]^2 + [y(t+\tau)-y(t)]^2\rangle$, where t is the elapsed time and τ is the time-lag or timescale, were calculated from the two-dimensional trajectories of the centroid of each nanosphere. Here, x and y are the time-dependent coordinates of the centroid of the particle. To compute a time-averaged MSD, one assumes that during the short movie-capture time of 20 seconds, no big change occurs in the micro-organization and micro-mechanical properties of the nucleus. This time invariance means that, on average, the MSD between, for example, 10 and 11 seconds is equal to that between 11 and 12 seconds. In this example, the time-lag τ is 1 second. We also report the ensemble-averaged MSD, $\langle\langle \Delta r^2(\tau)\rangle\rangle$, which represents the mean MSD and equals the sum of measured MSDs divided by the number of tracked nanospheres. Details about the method of particle-tracking microrheology can be found in (Tseng et al., 2002), who offer a thorough description of control experiments involving nanospheres of different size and surface charge.

Elastic and viscous moduli, $G'(\omega)$ and $G''(\omega)$, of the intranuclear region and cytoplasm were calculated from MSD measurements using the general method as described in (Tseng et al., 2002).

Shear flow experiments

Glass coverslips were cleaned and treated with 0.1-% poly-L-lysine (Sigma, St Louis, MO), and then coated with 20 μg/ml fibronectin (Calbiochem, San Diego, CA). Cells were seeded on those coverslips and allowed to grow for 24-48 hours before experimentation. Seeded coverslips were placed in a parallel-plate flow chamber (Glycotech,

Rockville, MD), which imposed calibrated shear flows, typically for 25-35 minutes, as indicated. The flow chamber was mounted on an inverted microscope (Nikon) and enclosed in an environmental chamber maintained at 37°C and 5% CO_2. Cells were verified to remain viable after application of the shear. The time-dependent positions of the nucleoli centroids were obtained using the particle-nanotracking system described above. The cell centroid was determined by tracing the edges of the cell, visualized by phase-contrast microscopy. The set of distances between nucleoli was used as a marker of structural coherence of the nucleus (Paddock and Albrecht-Buehler, 1986a; Paddock and Albrecht-Buehler, 1986b); the distance between cell centroid and nucleus centroid was used as a marker for the relative stiffness of cytoplasm and nucleus.

Non-specific binding to nanospheres

To assess the nonspecific binding of subcellular proteins to injected carboxylated nanospheres, we collected extracts of Swiss 3T3 fibroblasts lysates and incubated them for 24 hours in the presence of the particles. The resulting suspensions were separated by centrifugation and detected using SDS-PAGE electrophoresis with a sensitive sypro organe stain (Bio-Rad, Hercules, CA) and bicinchoninic acid (BCA) protein assay kit (Pierce Chemicals, Rockford, IL). A standard curve and equation for protein concentration vs absorbance was generated using the BCA assay on standard BSA samples of known concentration in concert with all unknown samples, and the measured absorbance at 562 nm were plotted against the known concentrations.

Results

We probe the mechanical behavior of the interphase nucleus in two different and complementary ways. First, we subject cells to controlled shear stresses and qualitatively examine the morphological response of cytoplasm, nuclear envelope, and intranuclear region. Next, we use the method of particle-tracking microrheology to measure the micromechanical and microstructural properties of the nucleus.

Morphological response of cytoplasm and nucleus to shear stresses

To characterize the mechanical behavior of cells, we assessed the morphological response of nucleus and cytoplasm to mechanical stresses. The time-dependent surface area of the nucleus and time-dependent perimeter and surface area of the sheared cells were monitored by time-lapsed phase-contrast microscopy. Interphase, adherent Swiss 3T3 fibroblasts were subject to shear flows generating a shear stress of 9.4 dyn/cm^2 (Fig. 1), using a parallel-plate flow chamber. This shear stress was sufficiently small not to detach the cells from their substratum. The plasma membrane of sheared cells exhibited large uncoordinated fluctuations (Fig. 1A and Movies 1-3, http://jcs.biologists.org/supplemental/). Consequently, the area of contact between the cells and their underlying substratum,

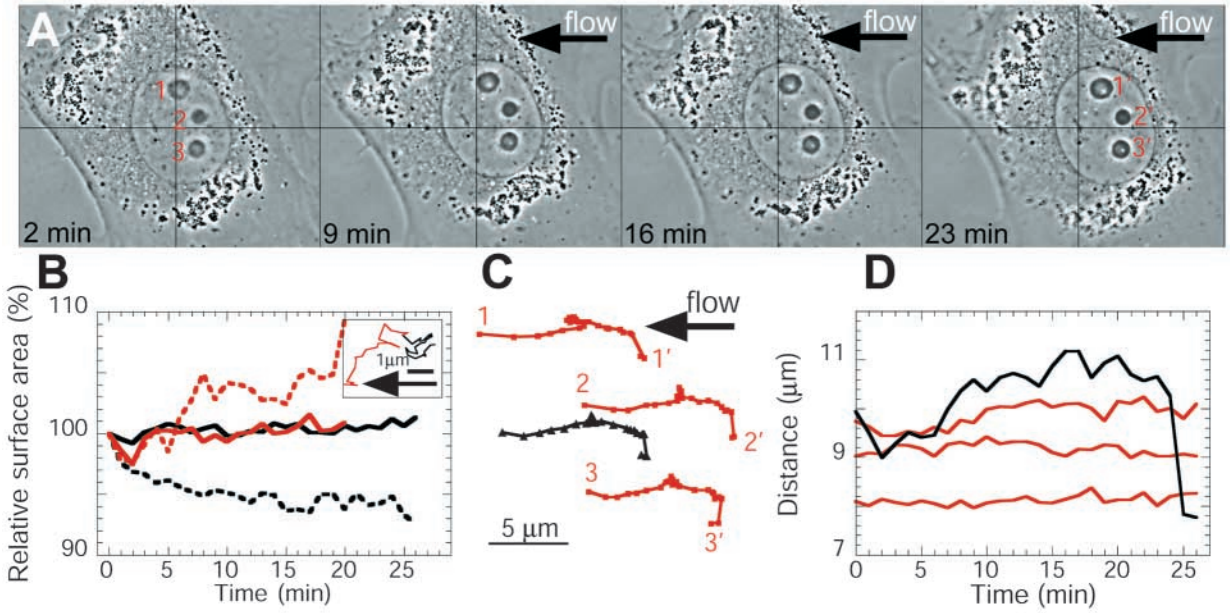

Fig. 1. Nuclei of cells under shear flow do not deform. (A) Four phase-contrast micrographs of Swiss 3T3 cells subject to a shear flow (wall shear stress=9.4 dyn/cm^2) taken over 23 minutes. Vertical and horizontal lines are guides to the eye. Cells were sheared for 27 minutes; arrows indicate the direction of flow. Three nucleoli are indicated. (B) Examples of relative surface areas of contact of two sheared cells with their substratum (dashed lines) and (apparent) surface areas of nuclei (solid lines) of the same sheared cells as a function of shearing time. The initial values of nucleus and cell surface areas are, respectively, 5100 μm^2 and 710 μm^2 for the cell shown in A (black lines; see movie M.2, http://jcs.biologists.org/supplemental/) and 4810 μm^2 and 350 μm^2 for the cell shown in movie M.3 (red lines). Surface areas were measured by morphometric analysis of phase-contrast micrographs of the cells under shear. Same colors correspond to the same cell. (Inset) Displacements of the centroids of sheared cells. Arrow indicates flow direction. This figure shows how cells can either move in the flow direction (black line) or counter-current (red line) (corresponding to cell shown in A). The starting point is where the two trajectories meet in the middle. (C) Typical movements of nucleoli centroids and nucleus centroid of a sheared cell (cell shown in A). In this particular case, nucleoli 1-3 and nucleus move from left to right (compare micrographs in A), and therefore move counter-current. The time lapse between symbols is 1 minute. 1-3 and 1′-3′, respectively, indicate start and end points of the trajectories. (D) Time-dependent distances between nucleoli centroids and the nucleus centroid (red lines) of a cell under shear and distance between cell centroid and nucleus centroid (black line) of the same sheared cell.

i.e. the cell footprint area, displayed positive and negative fluctuations that were as large as 12% of the initial cell footprint area (Fig. 1B, dashed lines). By contrast, the nucleus of sheared and unsheared cells displayed only minor fluctuations in shape (Fig. 1B, solid lines). The apparent surface area of the nucleus changed by at most 1.5% of the initial surface area of the nucleus during the same experimental time (Fig. 1B, solid lines; see also Movie 3).

Shear stresses induced net motion of the nucleus and the cytoplasm (Fig. 1A), as detected by the displacements of the cell centroid (Fig. 1B, inset) and the nucleus centroid (Fig. 1C, black line). Cell and nucleus moved frequently in opposite directions (Fig. 1B, inset), i.e. movements of cell and nucleus were partially uncoupled. Nucleoli moved in concert (Fig. 1C) and distances between nucleoli remained relatively constant. Hence, the coherence of the intranuclear region was not compromised by the applied shear stresses. The distance between nucleus centroid and cell centroid showed large fluctuations (Fig. 1D) that were mostly absent in no-shear conditions (Movie 4, http://jcs.biologists.org/supplemental/). Since materials respond to shear stresses according to their mechanical toughness, these results suggest that the cytoplasm is significantly softer than the nucleus. As described below, this result was confirmed independently and quantitatively using the method of particle tracking microrheology.

Mechanical response of cytoplasm and intranuclear region

The mechanical strength of the intranuclear region was qualitatively assessed by monitoring the time-dependent positions of the nucleoli and the centroids of the nuclei of the sheared cells. Fig. 1C illustrates how, under conditions of shear, nucleoli moved in concert. The movements of nucleoli followed no preferred direction with respect to the direction of overall cell motion. Accordingly, the distances between the nucleoli centroids (data not shown) and the distances between the nucleoli centroids and the nucleus centroid (Fig. 1D, red lines) varied little when shear forces were applied. These experiments suggest that not only is the nuclear envelope rigid, but also the intranuclear region. Together, the large excursions of the nucleus relative to the cytoplasm and the quasi-constant distance between nucleoli within the nucleus suggest that the perinuclear region of the cell deforms greatly under shear, while the nucleus remains stiff and undergoes rigid-body motion through the cytoplasm (Movies 1-3).

Spontaneous, random displacements of nanospheres in the intranuclear region

We quantified the mechanical properties and assessed the micro-organization of the intranuclear region using the method of multiple particle nanotracking (Apgar et al., 2000; Tseng et al., 2002). This approach probes the local viscoelastic properties and micro-organization of the nucleus in live cells by analyzing the MSDs of small inert nanospheres of known size and shape embedded in the nucleus. Fluorescent, 100-nm diameter nanospheres were microinjected directly into the nuclei of live cells. Subcellular position of the nanospheres in interphase cells was detected by constructing a three-dimensional image stack of combined fluorescence micrographs of the nanospheres and phase-contrast micrographs of the nuclear and plasma membranes, both collected in the same focal plane (Fig. 2). Different viewpoints on these stacks were obtained using custom image software for visual inspection of positions of nanospheres (Movie 5, http://jcs.biologists.org/supplemental/). Here, instead of measuring the mechanical response of the nucleus to applied shear-flow forces, the applied forces are very small local forces created by the spontaneous (thermal) fluctuations of the nanospheres. Intranuclear vs cytoplasmic location of the nanospheres was further verified by fluorescence microscopy by detecting the colocalization of the fluorescent nanospheres with DAPI-stained nuclear DNA (Fig. 2).

The spontaneous Brownian motion of nanospheres embedded in the intranuclear region and the cytoplasm of the same live cells was tracked with 5-nanometer and 33-millisecond resolutions by monitoring their centroid displacements with a video SIT camera (Fig. 3) (see Materials and Methods). The trajectories and shape of the MSD of the nanospheres embedded into the intranuclear region revealed novel physical and structural aspects of nucleus organization. Measured mechanical properties were highly reproducible, exhibiting cell-to-cell variations no larger than the differences between local moduli within a cell. Moreover, the transport of the nanospheres was verified to be purely Brownian, i.e. not directed, potentially by motor proteins or convective motion

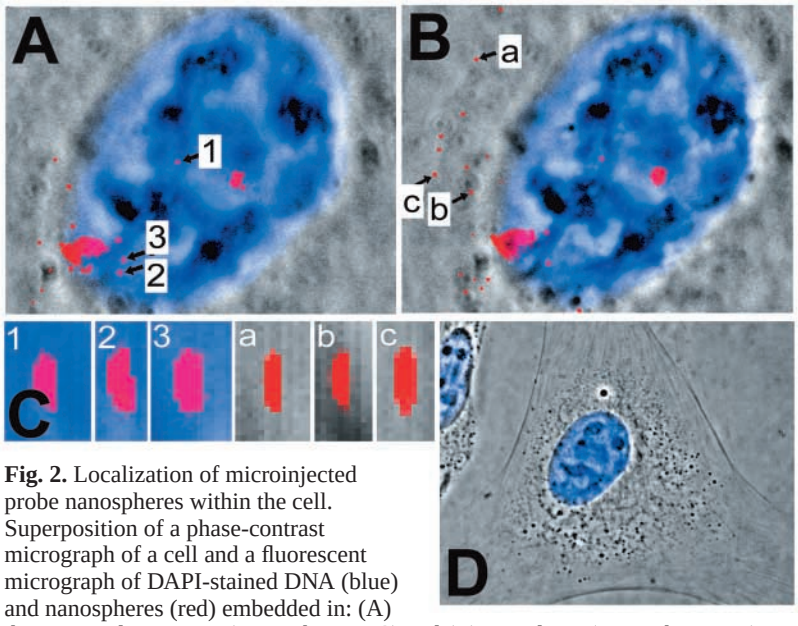

Fig. 2. Localization of microinjected probe nanospheres within the cell. Superposition of a phase-contrast micrograph of a cell and a fluorescent micrograph of DAPI-stained DNA (blue) and nanospheres (red) embedded in: (A) the intranuclear region (nanospheres 1-3) and (B) cytoplasm (nanospheres a-c). B was taken at a lower plane of focus than A. (C) Subcellular localization of nuclear (blue) and cytoplasmic (gray) nanospheres shown in A and B. Images represent composite images obtained by superimposing phase-contrast micrographs of the cell with fluorescent micrographs of the nanospheres and nuclear DAPI-stained DNA taken at different planes of focus. (D) Overall shape of the plasma membrane (phase contrast) and nucleus (blue DAPI stain) of the cells used in A-C.

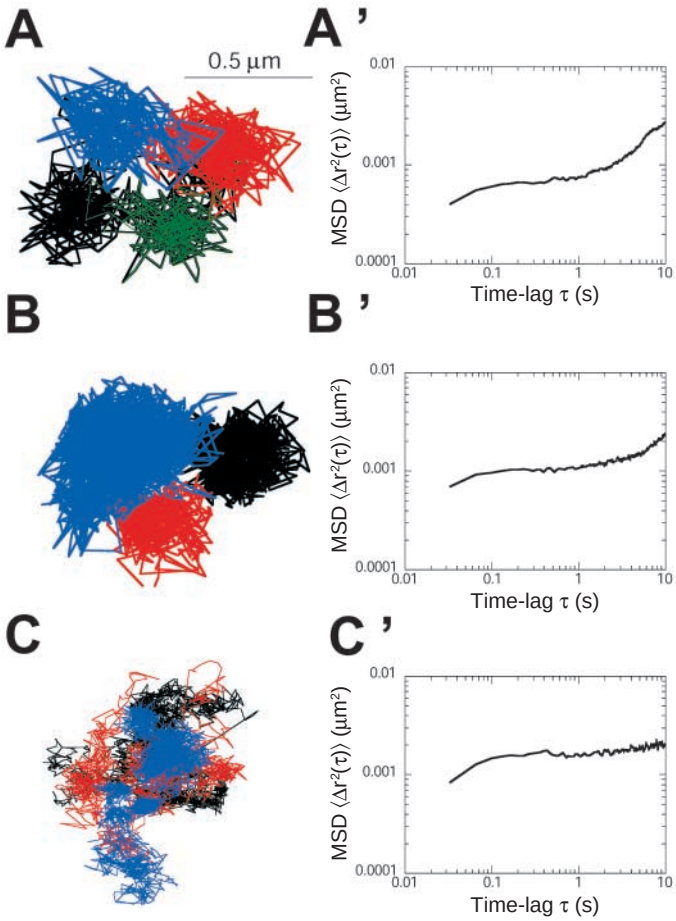

Fig. 3. Spontaneous movements of probe nanospheres embedded in the cytoplasm and the intranuclear region of the same cell. Typical trajectories of nanospheres embedded: (A) and (B) intranuclear region, (C) cytoplasm. (A'), (B') and (C') Associated MSDs, $\langle \Delta r^2(\tau) \rangle = \langle [x(t+\tau)-x(t)]^2+[y(t+\tau)-y(t)]^2 \rangle$.

within the nucleus. Indeed, unlike for Cajal bodies (Platani et al., 2002), PML nuclear bodies (Muratani et al., 2002) and endocytosed particles (Suh et al., 2003), the MSD of nanospheres microinjected in the cytoplasm and intranuclear region did not increase faster with time, a sign for directed motion. With little or no interactions with subnuclear structures and no directed motion, one can compute local elasticity and viscosity of the intranuclear region from measured displacements of the nanospheres (see below).

Nanospheres embedded in the intranuclear region often displayed segmented trajectories that were non-overlapping (Fig. 3A,B). In a manner reminiscent of the spontaneous movements of membrane proteins (Kusumi and Sako, 1996; Saxton and Jacobson, 1997), the nanospheres underwent movements that were briefly restricted to a small 'cage' before escaping to another cage for a longer period (Fig. 3A,B). To illustrate this caged motion, trajectories were color-coded (Fig. 3A,B). However, these cages are three-dimensional, whereas they are two-dimensional in the plasma membrane. Assuming that these cages are spherical, the diameter of a cage can be approximately obtained as the diameter of the nanosphere plus twice its mean displacement to the edge of the cage, i.e. $2a+2\langle \Delta r^2 \rangle_p^{1/2}$ (Fig. 4C). Here, $\langle \Delta r^2 \rangle_p$ is the value of the MSD in the plateau region evaluated at τ=1s (Fig. 4A,B, inset) and a=50 nm is the radius of the nanospheres. The mean diameter of these microdomains is 290±50 nm (mean±s.d., n=84) (Fig. 4C).

The MSD of the nanospheres in the nucleus showed a slight increase with time from 0 to 0.1 seconds, a quasi plateau at 0.1 to 1 seconds (motion bound by the cage boundaries) and a pronounced increase from 1 to 10 seconds (escape of the nanosphere from the cage) (Fig. 3A',B' and Fig. 4A,B, inset). The MSD profiles of nanospheres embedded in the cytoplasm (Fig. 3C') were similar to those of nanospheres embedded in the nucleus of the same cell (Fig. 3A',B'), displaying restricted motion at early time-points and viscous diffusion at later time-points. The averaged MSD, $\langle\langle \Delta r^2 \rangle\rangle$ showed a similar profile (Fig. 4B, inset) with a more pronounced curvature later in the time scale because of a few faster outliers. In startling contrast to nanospheres in the intranuclear region, most cytoplasmic nanospheres displayed overlapping, non-segmented trajectories and showed no 'caged-and-escape' motion (compare Fig. 3A and C).

The mean diffusion coefficient D of the nanospheres can be calculated from $\langle\langle \Delta r^2 \rangle\rangle$, because $D=\langle\langle \Delta r^2 \rangle\rangle/4\tau$ (Fig. 4D). The mean diffusion coefficient of the nanospheres decreased greatly with time-lag τ before reaching a plateau at later time-points (Fig. 4D). This signifies sub-diffusive transport at early time-points and free slow diffusion at later time-points (Fig. 4D). A slow camera would only capture this diffusive transport at later time-points. By contrast, the same nanospheres in water undergo free, fast and viscous diffusion, and their diffusion coefficient is constant with time and much higher (=4.53 µm²/second) (not shown).

Viscoelasticity of the intranuclear region and cytoplasm

The elastic and viscous moduli, $G'(\omega)$ and $G''(\omega)$, of the intranuclear region were directly obtained via Fourier/Laplace transformation of the mean MSD of nanospheres embedded in the intranuclear region (Fig. 5) (Mason et al., 1997). $G'(\omega)$ and $G''(\omega)$, respectively, characterize the elasticity (i.e. stiffness) and viscous modulus of the nucleus. The nucleus was very elastic (Fig. 5A): a simple description of the intranuclear region as a viscous liquid is incorrect. The elastic profile $G'(\omega)$ showed a steep frequency dependence at low frequencies before reaching a long plateau at intermediate and high frequencies (Fig. 5A). The viscous modulus G'' dominated the elastic modulus G' at low frequencies, became smaller than G' at intermediate frequencies and comparable to G' at high frequencies (Fig. 5A). This type of frequency profile signifies that the intranuclear region behaves as a viscoelastic solid ($G'>G''$) at high rates of deformations and as a viscoelastic liquid ($G'<G''$) at low rates of deformations.

These viscoelastic profiles, which are reminiscent of profiles found in polymeric networks (Ferry, 1980), describe the intranuclear region as a milieu, which does not relax when sheared rapidly and is therefore elastic, and which relaxes rapidly via viscous diffusion when sheared slowly, and therefore generates less resistance to mechanical stresses. The transition between these two regimes occurs at a time called the relaxation time, which is equal to the inverse of the frequency where $G'=G''$ (see more below) (de Gennes, 1991).

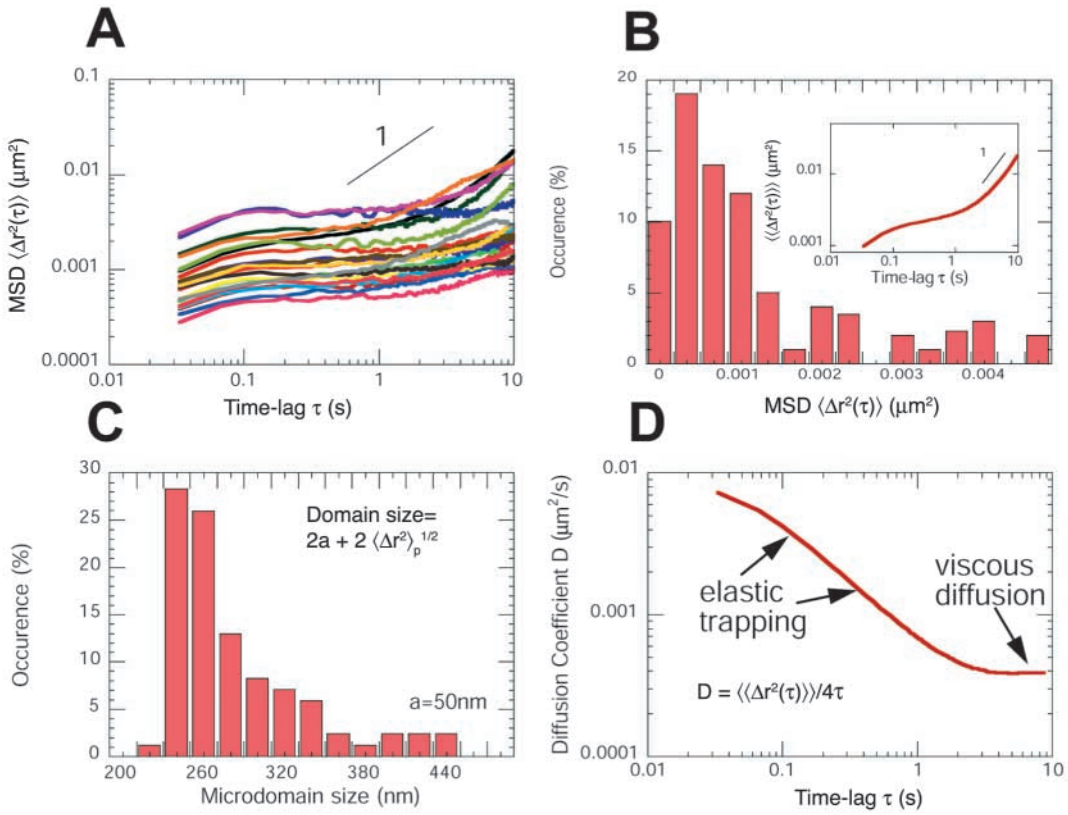

Fig. 4. Displacements of miscrospheres in the intranuclear region. (A) Typical MSD profiles of 100-nm diameter nanospheres in the intranuclear region. (B) Distribution of the MSDs of nanospheres embedded in the nucleus evaluated at a time-lag of 0.1 seconds. (Inset) Ensemble-averaged MSD of nanospheres embedded in the nucleus $\langle\langle\Delta r^2\rangle\rangle$ obtained by the sum of all MSDs and divided by the number of MSDs (n=84). (C) Size distribution of nuclear microdomains probed by particle nanotracking. The mean diameter is 290±50 nm (mean±s.d., n=84). (D) Mean diffusion coefficient, $D=\langle\langle\Delta r^2\rangle\rangle/4\tau$, of the nanospheres in the intranuclear region (n=84). At early time-points, D decreases with time, a sign for elastic trapping, whereas at later time-points, D becomes independent of time, a sign for viscous diffusion, albeit at a much slower pace than predicted by using the low interstitial viscosity measured by FRAP (see Discussion). The diffusion coefficient of the same nanospheres in water is constant and equals to 4.53 μm^2/second.

Using the same multiple-particle nanotracking method, we measured the viscoelastic properties of the cytoplasm of the same cells (Table 1). Right after microinjection of fluorescent nanospheres, some of them leach out into the perinuclear region (Fig. 2). Cytoplasmic viscoelastic moduli were significantly different from nuclear moduli. The stiffness, or plateau value of G′ (Fig. 5A), of the intranuclear region was about twofold higher than of the cytoplasm (Fig. 5A) (Tseng et al., 2002).The cytoplasm is thus significantly softer than the intranuclear region. The intranuclear region was also much more resilient against shear stresses than the cytoplasm. This is evident from the reduced crossover frequency of G′ and G″ and the much longer extent of the plateau modulus (G′ trace, Fig. 5A). The mean elasticity of the intranuclear region was 180 dyn/cm^2=18 Pa (plateau modulus). Finally, the intranuclear region was much more solid-like (i.e. more elastic than viscous) than the cytoplasm as measured by the phase angle [$=\tan^{-1}(G''/G')$] (Fig. 5A, inset). For comparison, the elasticity and phase angle of 1 mg/ml solutions of DNA (Mason et al., 1998), cytoplasmic F-actin (Palmer et al., 1999) and keratin (Yamada et al., 2003) are 0.02 dyn/cm^2 and 80°, 12 dyn/cm^2 and 30°, and 5 dyn/cm^2 and 10°, respectively.

The shear viscosity of the intranuclear region η_s sets the magnitude of the friction forces against which ATP-driven, directed movements of nuclear organelles occur (see Discussion for details). It can be shown that the shear viscosity of a complex fluid such as the intranuclear region is proportional to its plateau modulus and the relaxation time, $\eta_s = G'_p\tau_R$ (de Gennes, 1991). Here, G'_p is the plateau modulus (Fig. 5B, inset), which corresponds to the value of G′ where it is independent of frequency (for ω>1 Hz in Fig. 5A) and τ_R is the relaxation time (Fig. 5D, inset), which corresponds to the inverse of the frequency at which G′=G″(Fig. 5D) (de Gennes, 1991). Individual MSD profiles measured in the nucleus (n=84) were transformed into G′(ω) and G″(ω) profiles, from which τ_R, G'_p, and η_s were extracted. The viscosity of the intranuclear region ranged between 4 Poise (P) and 2200 P, with a mean of 520 P (Fig. 5D). For comparison, the viscosity of blood, corn syrup, molasses and ketchup at room temperature is ~0.1 P, ~20 P, ~50 P and ~500 P, respectively, whereas the viscosity of the fluid phase of the nucleus is ~0.01 P (Lukacs et al., 2000). The Discussion section shows how one can exploit knowledge of the viscosity of the nucleus to evaluate the diffusion coefficient of Cajal bodies and the propulsive forces required to direct the motion of PML bodies.

The degree of mechanical heterogeneity of the intranuclear

Table 1. Summary of the viscoelastic properties of the interphase nucleus

Shear viscosity η_s	Plateau modulus G'_p	Elastic modulus $G'(\omega)$	Phase angle δ
520 Poise	180 dyn/cm^2	135 dyn/cm^2 (1 Hz) 250 dyn/cm^2 (10 Hz)	24° (1 Hz) 36° (10 Hz)

Shear viscosity is estimated as the product of the plateau modulus and relaxation time. Relaxation time is the inverse of the frequency at which $G'=G''$ at low frequencies; the plateau modulus is the value of the elastic modulus when it flattens at intermediate frequencies. The phase angle is $\delta=\tan^{-1}(G''/G')$. All values correspond to mean values (n=84).

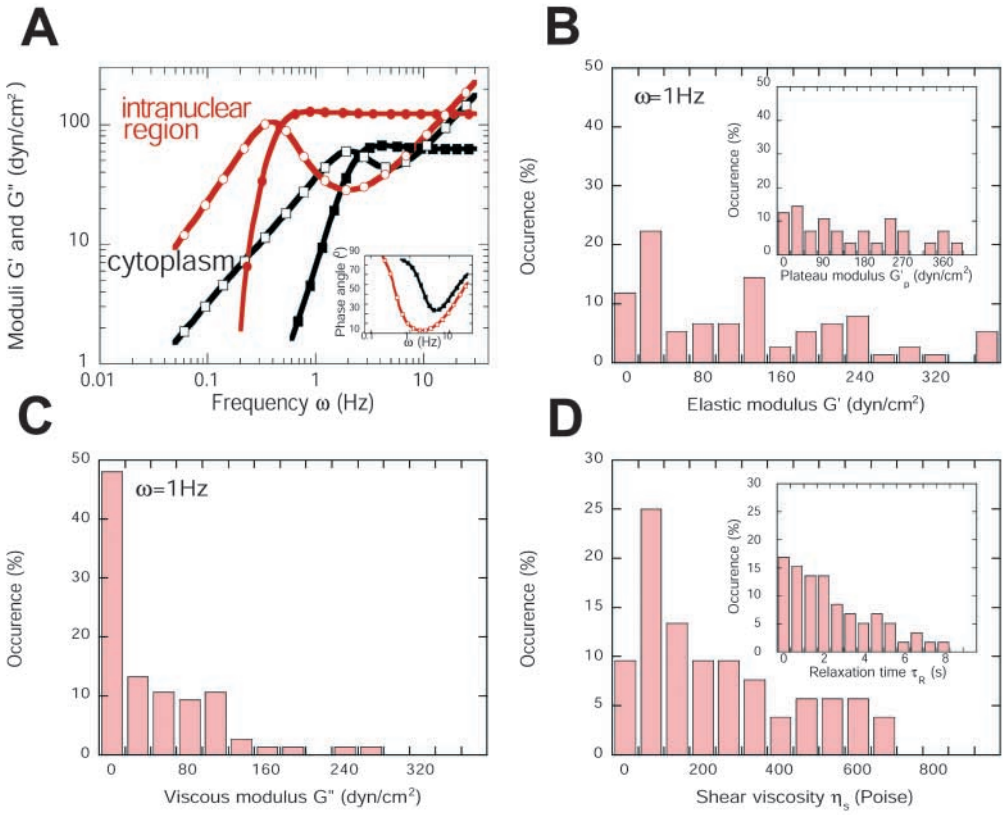

Fig. 5. Viscoelastic properties of the intranuclear region and the cytoplasm. (A) Mean frequency-dependent elastic [$G'(\omega)$] and viscous [$G''(\omega)$] moduli of the intranuclear region (black lines) and cytoplasm (red lines). Open symbols: G'; closed symbols: G''. (Inset) Frequency-dependent phase-angle for cytoplasm (black line) and intranuclear region (red line), $\delta(\omega)=\tan^{-1}[G''(\omega)/G'(\omega)]$. Examplary angles for liquids (e.g., glycerol), δ=90° and elastic solids (e.g. concrete), δ=0°. Mean moduli $G'(\omega)$ and $G''(\omega)$ were calculated from the ensemble-averaged MSD, $\langle\langle\Delta r^2(\tau)\rangle\rangle$, as described (Mason et al., 1997). Distribution of (B) elastic and (C) viscous moduli, G' and G'', respectively, in the intranuclear region measured at a frequency of 1 Hz. (D) Distribution of shear viscosity η_s [which is approximately the product of the plateau modulus G'_p (inset in B)] and the relaxation time τ_R (inset), $\eta_s=G'_p\tau_R$ (see text for details). For panels B-D, n=84; 1 Poise (P) = 1 Pascal second (Pa.s); 1 dyn/cm^2 = 0.1 Pa = 0.1 N/m^2.

region, as assessed by analyzing the distributions of elasticity (Fig. 5B), viscous modulus (Fig. 5C) and shear viscosity (Fig. 5D), was much higher than observed in homogenous solutions of glycerol (Apgar et al., 2000; Tseng et al., 2002) or reconstituted networks of chromosomal DNA (Goodman et al., 2002). These wide distributions demonstrate that the viscosity and elasticity of the nucleus cannot be described by single values.

Discussion

Interstitial and mesoscale viscosity of the nucleus

Together, shear-flow experiments and particle nanotracking measurements suggest that the intranuclear region is both highly viscous and elastic. FRAP and fluorescence correlation spectroscopy (FCS) applied to fluorescently-labeled nuclear proteins and polymers assume that the nucleus is only viscous and seemingly indicate that the viscosity of the nucleus is close to that of water (Lukacs et al., 2000; Pederson, 2000; Seksek et al., 1997). This apparent paradox can be explained by realizing that FRAP and FCS, which measure protein diffusion, are sensitive to the interstitial viscosity of the liquid phase of nucleus (the so-called nucleoplasm) and, presumably, the transient interactions that the probed molecules might have with nuclear binding partners (Lippincott-Schwartz et al., 2001; Misteli, 2001).

By contrast, the viscoelastic properties of nuclei measured here by nanotracking 100-nm nanospheres correspond to length scales larger than the effective mesh size of the cytoplasm and the intranuclear region. Hence particle

nanotracking measures the physical properties of the nucleus at the mesoscale, i.e. larger than the effective mesh size of the intranuclear region but still much smaller than the nucleus (Nickerson, 2001). The viscoelastic properties of isolated nuclei of chondrocytes have been determined using micropipette aspiration, which shows that nuclei behave as viscoelastic solid materials (Guilak et al., 2000). Such measurements complement our particle-tracking measurements, that analyze the viscoelasticity of the intranuclear region in live cells. As illustrated below, the mesoscale viscoelasticity of the nucleus determines the dynamics of nuclear organelles Cajal body and PML body. Therefore, FRAP/FCS and particle-tracking microrheology are complementary methods that measure viscoelastic properties of the intranuclear region at different length scales.

Viscoelasticity of the intranuclear region controls the movements of nuclear organelles and determines a lower bound for the forces required for their directed transport

Here, we show that the random and directed movements of nuclear organelles are affected by the mesoscale viscosity of the nucleus. The mean viscosity measured by particle tracking can be compared with that calculated from the diffusion coefficient of Cajal bodies in the intranuclear region of HeLa cells (Platani et al., 2002). Such a comparison is not straightforward because, unlike microinjected nanospheres which are monodisperse, Cajal bodies have a diameter varying by more than one order of magnitude (Gall, 2000); they also undergo random diffusion (free and constrained) and directed motion as demonstrated in Platani et al. (Platani et al., 2002). Moreover, the type of cells used in the studies of Platani et al. is different (Swiss 3T3 fibroblasts vs HeLa cells). The shear viscosity of the intranuclear region of HeLa cells can be estimated from the translational diffusion coefficient D of those Cajal bodies that undergo pure diffusion, $D=2\times10^{-2}$ μm^2/second–10^{-3} μm^2/second (Platani et al., 2002), and classical Stokes-Einstein relation as $\eta_s=k_BT/6\pi DR_{CB}$.

This relation assumes that Cajal bodies do not interact with nuclear structures. Here, R_{CB} is the radius of a Cajal body and is equal to 0.05-1 μm (Gall, 2000), k_B is the Boltzmann constant and equals to 1.38×10^{-23} J/K, and T is the temperature and equals to 310 K. Hence the apparent viscosity of the intranuclear region calculated from the diffusion coefficient of Cajal body is between 2.3 P (for R_{CB}=1 μm and $D=10^{-3}$ μm^2/second) and 230 P (for R_{CB}=0.05 μm and $D=2\times10^{-4}$ μm^2/second). These values compare favorably with those determined by particle tracking. Hence, the slow diffusion of Cajal bodies in the nucleus can be explained partially by the high mesoscale viscosity of the interphase nucleus. It is probable, however, that Cajal bodies interact with subnuclear structures which will affect its transport. Hence, particle tracking determines an upper bound of the diffusion coefficient of Cajal bodies.

When using the interstitial viscosity $\eta_s\approx0.01$ P measured by FRAP and FCS [that is 1.2 to 1.4 times the viscosity of water (Lukacs et al., 2000)], one finds diffusion coefficients of D=4.5 μm^2/second for R_{CB}=0.05 μm and 0.23 μm^2/second for R_{CB}=1 μm, that are much higher than observed experimentally. This result illustrates the fundamental difference between the interstitial viscosity, which controls the diffusion of small proteins within the nucleus, and the mesoscale viscosity, which affects the diffusion transport of nuclear organelles such as Cajal bodies.

Using the shear viscosity measured by particle tracking, we can also calculate the magnitude of the propulsive forces required to generate processive (not random) transport of PML bodies within the nucleus (Muratani et al., 2002). It has been speculated that the directed movement of PML bodies is consistent with the possibility that PML bodies act as nuclear sensors. Treatment of cells with the myosin inhibitor 2,3-butanedione monoxime reduces the speed of PML bodies (Muratani et al., 2002), suggesting that the motility of PML bodies is powered by a nuclear myosin (Pestic-Dragovich et al., 2000). Motile PML bodies have to overcome friction forces because of the viscosity of the intranuclear region. Hence, the minimal propulsive force required to generate directed motion of PML bodies is approximately given by the product of the friction coefficient of a PML body and its mean speed, $F \approx fv$.

Here, $f=6\pi\eta_sR_{PML}$ is the friction coefficient of a PML body, which is assumed to be spherical. Its radius R_{PML} is 0.1-0.5 μm (Zhong et al., 2000), η_s is the mean shear viscosity (measured by particle tracking of the intranuclear region) , the previously measured mean velocity of the fraction of motile PML bodies is v and equals to 4.3 μm/minute (Muratani et al., 2002). We find a force of F≈7-35 pico Newton (pN), which is relatively high compared with the force of ~1.6 pN generated by a single motor protein such as myosin I (Veigel et al., 1999). This force becomes much too high to be produced by motor proteins, considering the highest values of nuclear viscosity measured by us (2200 P). Hence, it is probable that PML bodies will follow paths through the intranuclear regions that correspond to regions of low viscosity. The distribution of local intranuclear viscosity is wide (Fig. 5D). When using the mean viscosity that corresponds to 75% of the lowest viscosity values (220 P), the force required to move these motile PML bodies is reduced to F≈3-15 pN. It is therefore probable, that each PML body is transported by multiple motor proteins working in concert. Of note, the diameter of PML bodies (0.2-1 μm) (Zhong et al., 2000) is similar or larger than the nuclear microdomains (0.29 μm) detected by particle nanotracking. When using the interstitial viscosity of the nucleus measured by FRAP and FCS, $\eta_s\approx0.01$ P, one finds a force of $1.4\text{-}6.8\times10^{-4}$ pN, which is several orders of magnitude too small to sustain the directed transport of nuclear organelles. Hence, the processive transport of PML bodies through the nucleus is directly affected by the mesoscale shear viscosity measured by particle tracking.

Interactions or large nuclear mesoscale viscosity?

The rapid transport of nuclear proteins seems well described by a hit-and-run model, where episodes of fast diffusion in the low-viscosity nucleoplasm are interrupted by relatively short-lived interactions with immobile obstacles in the nucleus (Phair and Misteli, 2001). Can a similar hit-and-run mechanism explain the slow diffusion of Cajal and PML bodies? We have just seen that, compared with nuclear proteins, the large size of these nuclear organelles does not explain their slow diffusion: The diffusion coefficient of nuclear organelles, calculated using the low interstitial viscosity of the nucleus, is too high by several orders of magnitude. Although one could describe the motion of nuclear organelles as short-lived rapid diffusion in the low-

viscosity nucleoplasm interrupted by strong, long-lived interactions with large nuclear obstacles. However, this paper shows that 100 nm latex particles do experience a huge viscosity. Therefore, nuclear particles of equal or larger size, such as PML and Cajal bodies, will experience the same large viscosity. These nanospheres display a slow diffusion, which is entirely explained by a high viscosity and high elasticity of the intranuclear region. Moreover, the extremely high mesoscale viscosity of the nucleus predicts correctly the diffusion coefficient of Cajal bodies and predicts propulsive forces for PML bodies of reasonable magnitude. These forces are within the range that is generated by a few putative nuclear motor proteins. In conclusion, whereas interactions between nuclear organelles and subnuclear structures are probably significant, especially in a regulatory role, the high mesoscale viscosity revealed by particle tracking contributes greatly in setting the pace of diffusion and the speed of directed transport of large macromolecular assemblies in the mammalian nucleus.

The authors thank Joseph G. Gall, Yixian Zheng, Kathy L. Wilson, Murray Stewart, Ben Schafer, and Maura Tumulty for insightful discussions. The authors acknowledge financial support from the National Science Foundation (NES/NIRT CTS0210718) and NASA (NAG9-1563).

References

Apgar, J., Tseng, Y., Federov, E., Herwig, M. B., Almo, S. C. and Wirtz, D. (2000). Multiple-particle tracking measurements of heterogeneities in solutions of actin filaments and actin bundles. *Biophys. J.* **79**, 1095-1106.

Bornfleth, H., Edelmann, P., Zink, D., Cremer, T. and Cremer, C. (1999). Quantitative motion analysis of subchromosomal foci in living cells using four-dimensional microscopy. *Biophys. J.* **77**, 2871-2886.

Carmo-Fonseca, M. (2002). The contribution of nuclear compartmentalization to gene regulation. *Cell* **108**, 513-521.

Cremer, T. and Cremer, C. (2001). Chromosome territories, nuclear architecture and gene regulation in mammalian cells. *Nat. Rev. Genet.* **2**, 292-301.

de Gennes, P.-G. (1991). Scaling concepts in polymer physics. Ithaca: Cornell University Press.

Edelmann, P., Bornfleth, H., Zink, D., Cremer, T. and Cremer, C. (2001). Morphology and dynamics of chromosome territories in living cells. *Biochim. Biophys. Acta* **1551**, M29-M39.

Ferry, J. D. (1980). Viscoelastic properties of polymers. New York: John Wiley and Sons.

Gall, J. G. (2000). Cajal bodies: the first 100 years. *Annu. Rev. Cell. Dev. Biol.* **16**, 273-300.

Gasser, S. M. (2002). Visualizing chromatin dynamics in interphase nuclei. *Science* **296**, 1412-1416.

Goodman, A., Tseng, Y. and Wirtz, D. (2002). Effect of length, topology, and concentration on the microviscosity and microheterogeneity of DNA solutions. *J. Mol. Biol.* **323**, 199-215.

Guilak, F., Tedrow, J. R. and Burgkart, R. (2000). Viscoelastic properties of the cell nucleus. *Biochem. Biophys. Res. Commun.* **269**, 781-786.

Kusumi, A. and Sako, Y. (1996). Cell surface organization by the membrane skeleton. *Curr. Opin. Cell Biol.* **8**, 566-574.

Lamond, A. I. and Earnshaw, W. C. (1998). Structure and function in the nucleus. *Science* **280**, 547-553.

Leduc, P., Haber, C., Bao, G. and Wirtz, D. (1999). Dynamics of individual flexible polymers in a shear flow. *Nature* **399**, 564-566.

Li, H. Y., Wirtz, D. and Zheng, Y. (2003). A mechanism of coupling RCC1 mobility to RanGTP production on the chromatin in vivo. *J. Cell Biol.* **160**, 635-644.

Lippincott-Schwartz, J., Snapp, E. and Kenworthy, A. (2001). Studying protein dynamics in living cells. *Nat. Rev. Mol. Cell Biol.* **2**, 444-456.

Luby-Phelps, K., Taylor, D. L. and Lanni, F. (1986). Probing the structure of cytoplasm. *J. Cell Biol.* **102**, 2015-2022.

Lukacs, G. L., Haggie, P., Seksek, O., Lechardeur, D., Freedman, N. and Verkman, A. S. (2000). Size-dependent DNA mobility in cytoplasm and nucleus. *J. Biol. Chem.* **275**, 1625-1629.

Marshall, W. F., Straight, A., Marko, J. F., Swedlow, J., Dernburg, A., Belmont, A., Murray, A. W., Agard, D. A. and Sedat, J. W. (1997). Interphase chromosomes undergo constrained diffusional motion in living cells. *Curr. Biol.* **7**, 930-939.

Mason, T. G., Dhople, A. and Wirtz, D. (1998). Linear viscoelastic moduli of concentrated DNA solutions. *Macromolecules* **31**, 3600-3603.

Mason, T. G., Ganesan, K., van Zanten, J. V., Wirtz, D. and Kuo, S. C. (1997). Particle-tracking microrheology of complex fluids. *Phys. Rev. Lett.* **79**, 3282-3285.

Misteli, T. (2001). The concept of self-organization in cellular architecture. *J. Cell Biol.* **155**, 181-185.

Muratani, M., Gerlich, D., Janicki, S. M., Gebhard, M., Eils, R. and Spector, D. L. (2002). Metabolic-energy-dependent movement of PML bodies within the mammalian cell nucleus. *Nat. Cell Biol.* **4**, 106-110.

Nickerson, J. (2001). Experimental observations of a nuclear matrix. *J. Cell. Sci.* **114**, 463-474.

Paddock, S. W. and Albrecht-Buehler, G. (1986a). The degree of coupling of nuclear rotation in binucleate 3T3 cells. *Exp. Cell. Res.* **166**, 113-126.

Paddock, S. W. and Albrecht-Buehler, G. (1986b). Distribution of microfilament bundles during rotation of the nucleus in 3T3 cells treated with monensin. *Exp. Cell. Res.* **163**, 525-538.

Palmer, A., Xu, J., Kuo, S. C. and Wirtz, D. (1999). Diffusing wave spectroscopy microrheology of actin filament networks. *Biophys. J.* **76**, 1063-1071.

Pederson, T. (2000). Diffusional protein transport within the nucleus: a message in the medium. *Nat. Cell Biol.* **2**, E73-E74.

Pederson, T. (2002). Dynamics and genome-centricity of interchromatin domains in the nucleus. *Nat. Cell Biol.* **4**, E287-E291.

Pestic-Dragovich, L., Stojiljkovic, L., Philimonenko, A. A., Nowak, G., Ke, Y., Settlage, R. E., Shabanowitz, J., Hunt, D. F., Hozak, P. and de Lanerolle, P. (2000). A myosin I isoform in the nucleus. *Science* **290**, 337-341.

Phair, R. D. and Misteli, T. (2000). High mobility of proteins in the mammalian cell nucleus. *Nature* **404**, 604-609.

Phair, R. D. and Misteli, T. (2001). Kinetic modelling approaches to in vivo imaging. *Nat. Rev. Mol. Cell Biol.* **2**, 898-907.

Platani, M., Goldberg, I., Lamond, A. I. and Swedlow, J. R. (2002). Cajal body dynamics and association with chromatin are ATP-dependent. *Nat. Cell Biol.* **4**, 502-508.

Politz, J. C., Browne, E. S., Wolf, D. E. and Pederson, T. (1998). Intranuclear diffusion and hybridization state of oligonucleotides measured by fluorescence correlation spectroscopy in living cells. *Proc. Natl. Acad. Sci. USA* **95**, 6043-6048.

Politz, J. C., Tuft, R. A., Pederson, T. and Singer, R. H. (1999). Movement of nuclear poly(A) RNA throughout the interchromatin space in living cells. *Curr. Biol.* **9**, 285-291.

Politz, J. C., Yarovoi, S., Kilroy, S. M., Gowda, K., Zwieb, C. and Pederson, T. (2000). Signal recognition particle components in the nucleolus. *Proc. Natl. Acad. Sci. USA* **97**, 55-60.

Saxton, M. J. and Jacobson, K. (1997). Single-particle tracking: applications to membrane dynamics. *Annu. Rev. Biophys. Biomol. Struct.* **26**, 373-399.

Seksek, O., Biwersi, J. and Verkman, A. S. (1997). Translational diffusion of macromolecule-sized solutes in cytoplasm and nucleus. *J. Cell Biol.* **138**, 131-142.

Suh, J., Wirtz, D. and Hanes, J. (2003). Efficient active transport of gene nanocarriers to the cell nucleus. *Proc. Natl. Acad. Sci. USA* **100**, 3878-3882.

Tseng, Y., Kole, T. P. and Wirtz, D. (2002). Micromechanical mapping of live cells by multiple-particle-tracking microrheology. *Biophys. J.* **83**, 3162-3176.

Tseng, Y. and Wirtz, D. (2001). Mechanics and multiple-particle tracking microhetrogeneity of alpha-actinin-cross-linked actin filament networks. *Biophys. J.* **81**, 1643-1656.

Vazquez, J., Belmont, A. S. and Sedat, J. W. (2001). Multiple regimes of constrained chromosome motion are regulated in the interphase Drosophila nucleus. *Curr. Biol.* **11**, 1227-1239.

Veigel, C., Coluccio, L. M., Jontes, J. D., Sparrow, J. C., Milligan, R. A. and Molloy, J. E. (1999). The motor protein myosin-I produces its working stroke in two steps. *Nature* **398**, 530-533.

Yamada, S., Wirtz, D. and Coulombe, P. A. (2003). The mechanical properties of simple epithelial keratins 8 and 18: discriminating between interfacial and bulk elasticities. *J. Struct. Biol.* **143**, 45-55.

Zhong, S., Salomoni, P. and Pandolfi, P. P. (2000). The transcriptional role of PML and the nuclear body. *Nat. Cell Biol.* **2**, E85-E90.